RESEARCH ARTICLE | SEPTEMBER 20 2023

Near-zero-power infrared relay based on microfluidic switch and metamaterial absorber

Zekun Zhang ; Jiawen Yan ; Jiahao Zhao; Peng Li

Appl. Phys. Lett. 123, 123507 (2023)
https://doi.org/10.1063/5.0168979

Applied Physics Letters ARTICLE pubs.aip.org/aip/apl

Near-zero-power infrared relay based on microfluidic switch and metamaterial absorber

Cite as: Appl. Phys. Lett. **123**, 123507 (2023); doi: 10.1063/5.0168979
Submitted: 21 July 2023 · Accepted: 8 September 2023 ·
Published Online: 20 September 2023

Zekun Zhang,[1,2,3] Jiawen Yan,[1,2,3] Jiahao Zhao,[1,2,3] and Peng Li[1,2,3,a)]

AFFILIATIONS

[1]State Key Laboratory of Precision Measurement Technology and Instruments, Department of Precision Instruments, Tsinghua University, Beijing 100084, China
[2]Key Laboratory of Smart Microsystem (Tsinghua University) Ministry of Education, Beijing 100084, China
[3]Beijing Advanced Innovation Center for Integrated Circuits, Beijing 100084, China

[a)]**Author to whom correspondence should be addressed:** pengli@mail.tsinghua.edu.cn

ABSTRACT

Internet of Things sensor nodes, which integrate information acquisition, processing, exchange, and execution modules, have widely been used for unattended industrial production, environmental monitoring, and other fields. However, limited battery power constrains the lifespan of the sensor nodes. In this paper, we propose a near-zero-power infrared relay consists of microfluidic switches and a metamaterial absorber (MA). When target appears, the MA absorbs the infrared energy emitted from the target and uses it to turn on the microfluidic switch. When valid information is not present, the microfluidic switch is in "off" state with a high resistance of over 10^9 Ω. The infrared relay with a pair of microfluidic switches shows common mode suppression capability against environmental temperature variation. We further demonstrate a sensor node consists of the infrared relay and a MoS_2 photodetector. In a standby mode, the sensor node shows near-zero power consumption. As target infrared signal occurs, the photodetector is wakened by the infrared relay and illustrates excellent optical sensing performance. The simplicity of this approach provides a route for significantly extending the lifespan of sensor nodes powered by batteries, especially the sensor nodes for detecting infrequent but critical events.

With the ongoing revolution of the Internet of Things (IoT), the development of related intelligent sensing technologies has resulted in billions of smart sensor nodes that greatly aid industrial, agricultural, and environmental monitoring.[1–4] However, their significant energy consumption has also created a substantial burden on energy supply and environmental sustainability.[5,6] Sensor nodes deployed for fieldwork often face the challenge of obtaining a reliable power supply, which makes their batteries the primary limiting factor for the lifespan of the sensor nodes.[7] This issue is especially important when detecting infrequent but critical events, such as forest fires and gas leaks.[8,9] Since the sensor node needs to continuously consume electrical power, most of the battery power is consumed without acquiring any useful information.[9–11]

Sensor nodes integrated with nanogenerator have the potential to extend their operational lifespan by energy harvesting. However, energy from environment, such as vibration energy, is not guaranteed to be available when required. Another approach of extending lifespan of sensor nodes is using energy management strategies. Energy management strategies need to be tailored to the specific power supply methods, such as Li-batteries and supercapacitors. Liu *et al.* employed a dynamic programming algorithm to plan the energy allocation between lithium batteries and supercapacitors.[12] It conforms to the working characteristics of the sensor node and maximizes its lifetime. However, the standby power consumption cannot be completely eliminated. Researchers also explored various wake-up approaches to reduce the standby power. Zhu *et al.* developed a low power RF wake-up receiver based on an AlN RF resonant switch.[13] As a 1 GHz signal modulated at 100 kHz passed through the resonator, the RF signal was amplified to activate the receiver module. This device can only be awakened by RF radio signals, which limits its application. Bannoura *et al.* utilized a microphone to detect sound from target and converted it to wake-up signal by a module comprising filter, amplifier circuits, and microcontroller.[14] Rosa *et al.* developed a MEMS piezoelectric transducer, which generated voltage signal as vibration is detected.[15] Dudko and Overmeyer developed an optical wake-up approach.[16] A solar cell was used to produce voltage signals to control the power management circuit. All these wake-up approaches need circuit to generate wake-up signal. Although low-power CMOS circuits are

applied, they cannot completely eliminate standby power consumption. Therefore, the sensor nodes, which only consumes energy when target is present, are desired.

Qian *et al.* utilized the thermal effect of an infrared metamaterial absorber (MA) to convert infrared energy emitted from the target into heat, which drove a microcantilever beam to bend downward and contacted with a metal electrode, achieving a near-zero-power infrared digitizer with almost no power consumption in a standby mode.[17–19] However, the near-zero-power infrared digitizer faces challenges, such as difficult fabrication and easy spurious triggering. Additionally, the infrared digitizer was not self-holding, and it turned off immediately after the infrared signal disappeared. As a result, the sensor node may not have enough time to finish information acquisition, processing, exchange, and execution process before turning off. As such, reliable, easily fabricated, and self-holding near-zero-power sensor nodes are highly desired.

In this work, we demonstrated an infrared relay based on a MA and a pair of microfluidic switches. As target appeared, the MA integrated in the microfluidic switch absorbed infrared energy and converted it into heat. Owing to the thermal insulation structure we designed, most of the heat from MA can be used to turn on the microfluidic switch. As target disappeared, the self-holding microfluidic switch slowly turned off. The design of a symmetric pair of microfluidic switches largely reduced the influence of ambient temperature variation.

Figures 1(a) and 1(b) are the schematic views of the infrared relay, which is composed of two symmetrical thermal actuated microfluidic switches. Each microfluidic switch consists of a liquid reservoir, a 30 μm-wide microchannel, and metal electrode arrays. The reservoir and partial of the microchannel were first filled with 0.19 ml kerosene (supplied by Macklin) as an insulating liquid, and then a trace of ferric chloride solution (~0.14 nl) was filled into the microchannel as the conductive liquid. The detailed liquid filling method is shown in the supplementary material. The MA was completely immersed in kerosene in the reservoir. The infrared signal that matched the absorption spectrum of MA passed through an infrared transmissive calcium fluoride window and illuminated the MA. The heat generated caused the expansion of the kerosene in the reservoir. By connecting a microchannel to the reservoir, we converted the tiny volume expansion of kerosene into large displacement. The liquid displacement Δx is

$$\Delta x = \frac{\Delta V}{A}, \tag{1}$$

where ΔV is the expansion volume, and A is the cross-sectional area of the microchannel. As the absorbed energy exceeds a certain threshold, the ferric chloride conductive solution is connected to the proper set of electrodes to turn on the infrared relay [Fig. 1(d)]. According to our simulation results, Δx is approximately 600 μm. The electrode width and gap are both 300 μm, so that the $FeCl_3$ solution can bridge proper set of electrodes. Under environmental temperature variation, the ferric chloride solutions in both microchannels move simultaneously without turning on the infrared relay, demonstrating common mode suppression capability against environmental temperature variation, as shown in Fig. 1(e).

MA can effectively absorb infrared signals with excellent frequency selectivity.[20,21] Therefore, the near-zero-power relay can only be turned on by infrared signal with specific frequency (or wavelength). The MA was composed of metal antenna arrays, silicon nitride dielectric layer, and bottom metal reflective layer.[22–24] Due to the bottom metal reflective layer, the transmittance of MA is

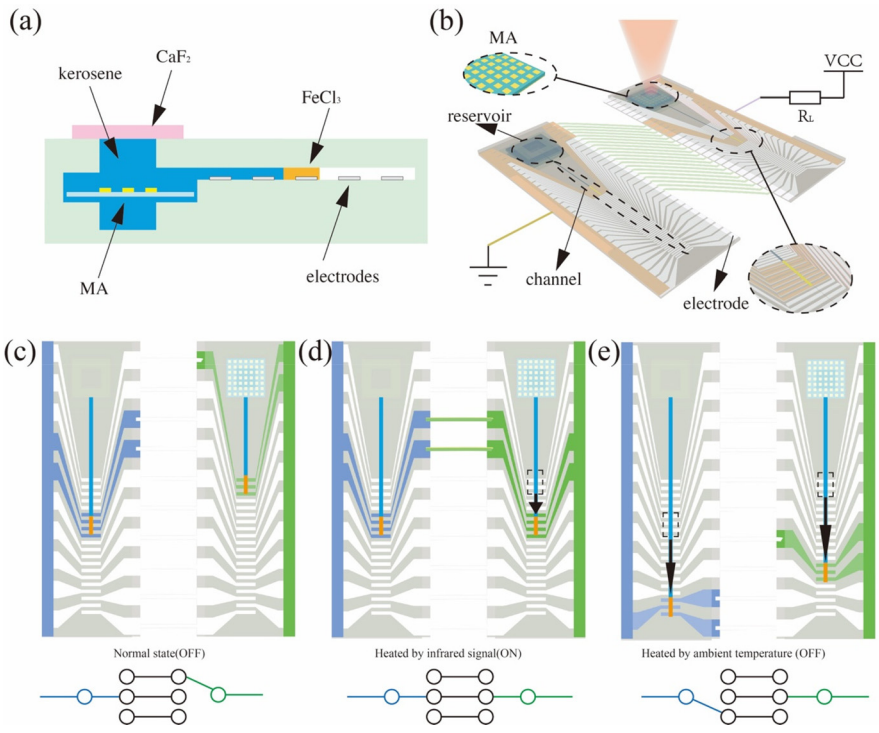

FIG. 1. Infrared relay. (a, b) Schematic views of the infrared relay with MA and a pair of microfluidic switches. (c) The infrared relay in "off" state. (d) The heat generated from MA causes the expansion of the kerosene in reservoir and large displacement of ferric chloride solution in the microchannel. As absorbed energy exceeds a certain threshold, the ferric chloride solution bridges the proper set of electrodes and turns on the relay. (e) Under environmental temperature variation, ferric chloride solutions in both microchannels move simultaneously without turning on the infrared relay.

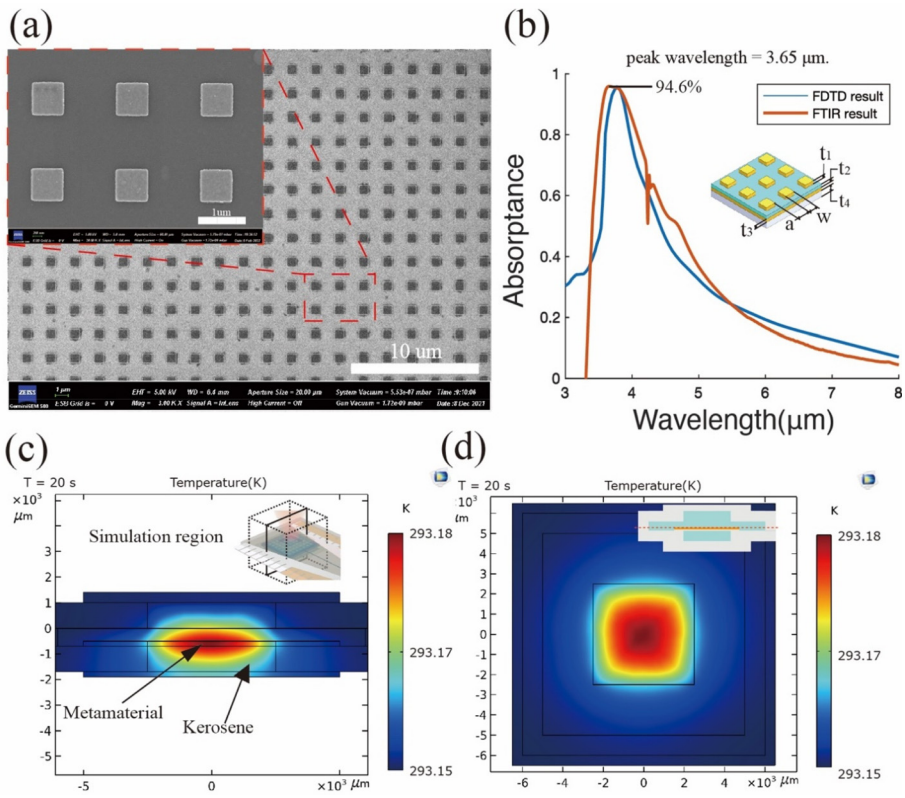

FIG. 2. (a) SEM image of MA. (b) The absorption spectra of the MA (FDTD simulation result and experimental result) and schematic view of the MA. (c) Simulation result of the temperature distribution in the vertical cross section after 20 s of heating. (d) Simulation result of the temperature distribution in the horizontal cross section after 20 s of heating.

negligible. In order to achieve excellent absorption capability, the effective impedance of MA should match the free space impedance

$$\sqrt{\mu(\omega)/\epsilon(\omega)} = Z_0, \tag{2}$$

where $\mu(\omega)$ is magnetic permeability, $\epsilon(\omega)$ is the permittivity, Z_0 is the characteristic impedance of free space, and ω is frequency. As two metallic layers have strong magnetic resonance under the incidence wave, a significant enhancement of the localized electromagnetic field is established in the Si_3N_4 layer. Consequently, electromagnetic energy can be efficiently confined in MA and converted to heat. We designed a mid-infrared MA with a sharp absorption peak at wavelength of 3.65 μm utilizing a finite difference time domain (FDTD) method. The surface area of MA was $5 \times 5\,\text{mm}^2$. The surface morphology of as-fabricated MA was characterized using scanning electron microscopy (SEM) as shown in Fig. 2(a). The linewidth error of fabrication was less than 20 nm. Important design parameters of MA are listed in Table I and Fig. 2(b). The absorption spectrum of MA was characterized using Fourier transform infrared spectroscopy (FTIR), which exhibited a high absorption rate of 94.6% at wavelength of 3.65 μm with a full width at half maximum (FWHM) of 1.3 μm, indicating excellent infrared signal absorption capability and frequency selectivity. The experimental results matched with our simulation results [Fig. 2(b)].

Kerosene in reservoir absorbed the heat generated from MA, resulting in volume expansion. The kerosene volume expansion ΔV can be expressed as

$$\Delta V = \frac{\alpha}{Cm} Q, \tag{3}$$

where α is thermal expansion coefficient of kerosene, C is the heat capacity, m is the mass of the kerosene, and Q is the heat absorbed by kerosene. Volume expansion ΔV is in proportional with the heat absorbed. Since the infrared energy emitted from target is usually extremely low, thermal insulation is essential to minimize heat dissipation and make fully use of the energy absorbed by MA. To minimize heat dissipation, we selected sodium-calcium glass as a substrate material due to its low thermal conductivity of 0.81 W/mK. We immersed MA into kerosene. Owing to the ultralow thermal conductivity of kerosene (0.2 W/mK), the heat generated from MA was mainly absorbed by kerosene instead of glass substrate. In addition to ultralow thermal conductivity, another important advantage of kerosene is its high

TABLE I. Geometry parameters of MA.

Parameters	Description	Design (μm)
a	Spacing between metal antennas	1.13
w	Width of metal antenna	0.77
t_1	Thickness of metal antenna	0.05
t_2	Thickness of Si_3N_4	0.3
t_3	Thickness of bottom metal layer	0.05
t_4	Thickness of glass substrate	200

infrared transmittance (~100%, see the supplementary material). As such, infrared signals can pass through kerosene layer and illuminate MA.

The simulation of temperature distribution in the reservoir (20 s after infrared illumination) was performed by the finite element method via COMSOL Multiphysics. The power density of MA was set to 12.5 W/m^2. As shown in Figs. 2(c) and 2(d), the temperature rise was concentrated around MA, and glass substrate demonstrated almost no temperature change. According to our simulation results, 60% of the heat generated from MA was directly absorbed by kerosene due to its excellent thermal insulation capability. Thermal insulation capability of kerosene largely reduces the heat dissipation rate, which is also important for self-holding capability.

The heat generated from MA resulted in the expansion of kerosene in reservoir, thereby solution in the microchannel was pushed to move forward. Two immiscible solutions are desired to realize two-phase flow in the microchannel. Kerosene is insulating oily solution, and ferric chloride solution is chosen as conductive aqueous liquid. Under temperature variation of 0.2 °C, back-and forth displacement of 4038 μm of the two-fluid interface was observed for more than ten cycles (see the supplementary material). In order to achieve reliable switching performance, it is crucial to maintain the stability of the two-phase flow and prevent mixing of the two types of liquids during the kerosene expansion/contraction. Han *et al.* deduced a relation between the thickness of residual liquid δ on sidewall and channel width w for noncircular microchannels:[25]

$$\delta \sim \frac{\sqrt{2}\left(\frac{\mu U}{\sigma}\right)^{\frac{2}{3}} \frac{2wh}{w+\sqrt{w^2+4h^2}}}{\left(\frac{\mu U}{\sigma}\right)^{\frac{2}{3}} + \left(1 - \frac{\rho U^2\left(\frac{\sqrt{2}wh}{w+\sqrt{w^2+4h^2}} - \delta_{corner}\right)}{\sigma}\right)^{\frac{2}{3}}}, \quad (4)$$

where μ is the dynamic viscosity of the liquid, U is the characteristic velocity, σ is the surface tension or interfacial tension between the two fluid phases, ρ is the liquid density, and h is the height of channel. It indicates that the channel with small width w can largely reduce the amount of liquid left on the sidewall during liquid movement. Smaller channel width also leads to smaller Reynolds number, which can prevent the occurrence of turbulent flow. We tested microchannels with different diameters of 120, 91, 47, and 29 μm. As shown in Fig. 3, a clear residual liquid on sidewall and mixing of kerosene and ferric chloride solution usually occurred in channels wider than 40 μm during the liquid movement. Therefore, it is difficult to realize microfluidic switch based on two-phase flow by using these microchannels. In the 29 μm wide microchannel [Fig. 3(d)], the two-phase flow kept stable during liquid movement. Therefore, microchannels narrower than 30 μm were chosen for our devices.

Then, we investigated the characteristics of infrared relay consisted of MA and microfluidic switches by using a digital multimeter (Keysight 34470). The experiments were carried out under atmospheric pressure at room temperature. A 170-mW blackbody light source with a calcium fluoride filter was utilized as an infrared source to irradiate the relay. Below the relay, a microscope recorded the movement of liquid in the microchannel. Figures 4(a) and 4(b) illustrate the characteristics of a single microfluidic switch integrated with

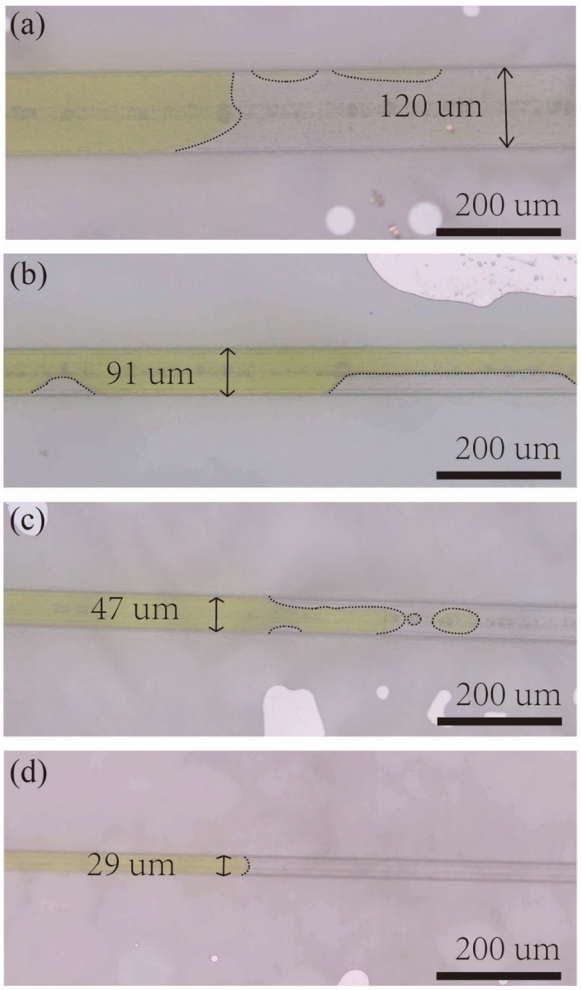

FIG. 3. (a) Kerosene and ferric chloride solution in microchannels with a width of 120 μm. (b) Kerosene and ferric chloride solution in microchannels with a width of 91 μm. (c) Kerosene and ferric chloride solution in microchannels with a width of 47 μm. (d) Kerosene and ferric chloride solution in microchannels with a width of 29 μm. Mixing of kerosene and ferric chloride solution usually occurs in channels wider than 40 μm during the liquid movement.

MA. Under 3.65 μm infrared illumination, the microfluidic switch turned on within ~15 s and slowly turned off as the infrared source was removed [Fig. 4(a)], demonstrating excellent switching performance with good repeatability. The resistance of the device in the "on" state is approximately 396 kΩ. It should be noted that the upper detection limit of the digital multimeter is 1 GΩ, so the actual "off" state resistance of our microfluidic switch surpasses 1 GΩ. The I–V curves demonstrate that the "off" state resistance is 44.3 GΩ (see the supplementary material). The same device showed negligible response to 0.65 μm illumination [Fig. 4(b)], indicating good frequency selectivity. The measured leakage current value of 20 nA is a result of the noise from the measuring instrument. Figures 4(c) and 4(d) illustrate the characteristics of a single microfluidic switch without MA in reservoir. The device showed no response to 3.65 μm infrared illumination and

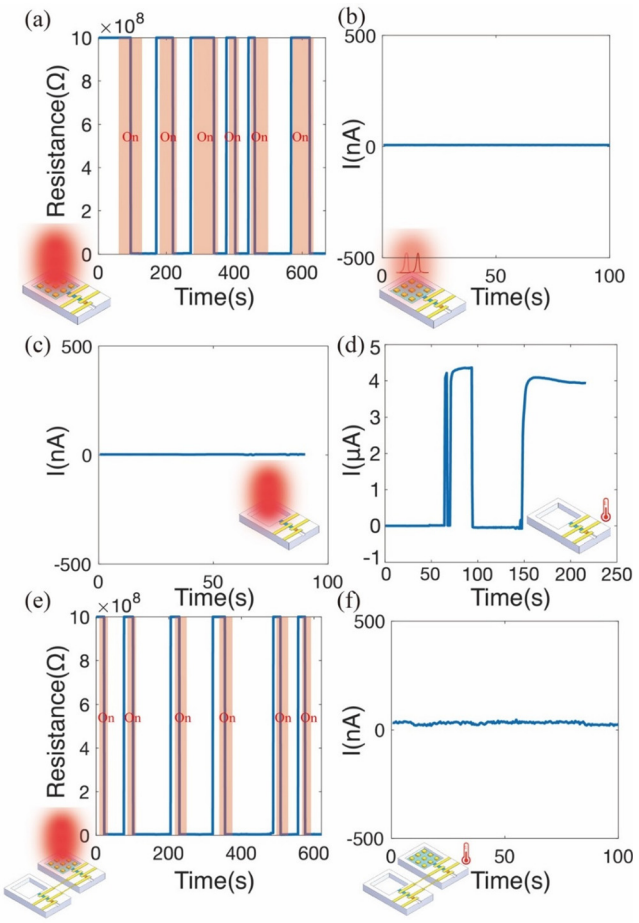

FIG. 4. (a) Single microfluidic switch with MA under 3.65 μm infrared irradiation. (b) Single microfluidic switch with MA shows negligible response to 0.65 μm illumination, indicating good frequency selectivity. (c) Single microfluidic switch without MA shows negligible response to 3.65 μm infrared irradiation. (d) Single microfluidic switch (without MA) under ambient temperature variation. (e) Infrared relay composed of a pair of microfluidic switches under 3.65 μm infrared irradiation. (f) Infrared relay composed of a pair of microfluidic switches under ambient temperature variation.

maintained a high-resistance state. The device with only one microfluidic switch is very sensitive to ambient temperature variation. It easily turned on and off as temperature changed within ~1 °C [Fig. 4(c)]. Figures 4(e) and 4(f) illustrate the characteristics of an infrared relay composed of a pair of microfluidic switches, and only one switch is integrated with MA. The relay showed clear response to 3.65 μm infrared illumination. It turned on within ~15 s and slowly turned off after ~100 s as the infrared source was turned off, which demonstrated excellent switching performance with self-holding capability. The power needed to activate the circuit depends on the original position of the two-fluid interface between the electrodes. The largest infrared power needed to activate the circuit is 0.8 μW. Figure 4(f) shows that the infrared relay kept "off" state as ambient temperatures increased (~1 °C), indicating that the symmetric pair of microfluidic switches largely reduced the influence of ambient temperature variation. The main source of uncertainty results from measuring instrument due to the extremely high "off" state resistances and extremely low "off" state currents. We tested the devices under various conditions. They were exposed to visible light with different intensities and tested under various temperatures. The devices demonstrated excellent switching performance (see the supplementary material).

Finally, we demonstrated a near-zero-power optical sensing node, which consisted of the infrared relay and a MoS_2 photodetector [Fig. 5(a)]. The manufacturing process of the MoS_2 photodetector is shown in the supplementary material. In the absence of infrared signal, the infrared relay kept "off" state with high resistance to realize near-zero power consumption, and the MoS_2 photodetector had no response to (520 nm) visible light. As infrared signal was applied, the relay switched to the "on" state. The MoS_2 photodetector was waken up and demonstrated a clear sensitivity to visible light illumination. The resistance of the MoS_2 photodetector decreased under 520 nm illumination and rapidly changed back to the original value as the visible light was turned off, demonstrating excellent repeatability [Fig. 5(b)]. As the infrared signal was removed, the sensing node slowly switched to "off" state. Our optical sensing node demonstrated excellent near-zero-power sensing capability.

In conclusion, we demonstrated a near-zero-power infrared relay based on MA and microfluidic switches. The infrared relay can convert (3.65 μm) infrared signals emitted from target into heat by MA and use the heat to turn on the microfluidic switch. We further realized a near-zero-power optical sensing node, which consisted of the infrared relay and a MoS_2 photodetector. Compared with various wake-up approaches previously reported, our relay has almost no power consumption in the standby mode. Compared with Qian's near-zero-power infrared digitizer, our device is easier to fabricate. The metamaterial absorber and microfluid switch can be fabricated separately and then assembled. Additionally, our relay is not easy for spurious triggering and has self-holding capability. Our strategy can significantly extend the lifespan of sensor nodes powered by batteries, especially the sensor node for detecting infrequent but critical events. The near-zero-power relay can be applied in various fields, including smart agriculture (plant irrigation and pest detection), environment monitoring (wildfires and gas leakage detection), and automated industrial production inspection.

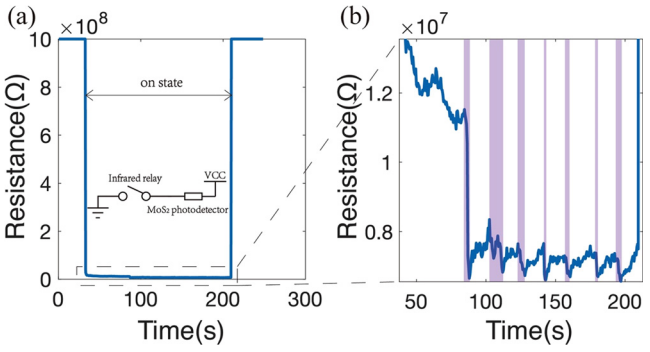

FIG. 5. (a) Characteristic of the near-zero-power optical sensing node, which consisted of the infrared relay and a MoS_2 photodetector. (b) Zoom in view of the response of the MoS_2 photodetector to visible light as the infrared relay is in the "on" state (the purple area indicates that the visible light is turned on).

See the supplementary material for details regarding MA fabrication, fabrication of microfluidic switch, transmission of Kerosene, back-and-forth motion of two-fluid interface, I–V characteristic curve of the device in "off" and "on" state, devices performance under various conditions, and fabrication of the MoS_2 photodetector.

This work was supported by the National Natural Science Foundation of China (Nos. 52322512 and 51775306) and the Beijing Municipal Natural Science Foundation (No. 4192027).

AUTHOR DECLARATIONS

Conflict of Interest

The authors have no conflicts to disclose.

Author Contributions

Zekun Zhang: Investigation (lead); Methodology (equal); Writing – original draft (lead). **Jiawen Yan:** Data curation (equal); Writing – review & editing (equal). **Jiahao Zhao:** Investigation (equal); Resources (equal). **Peng Li:** Funding acquisition (lead); Investigation (lead); Methodology (equal); Resources (equal); Supervision (lead); Writing – review & editing (equal).

DATA AVAILABILITY

The data that support the findings of this study are available from the corresponding author upon reasonable request.

REFERENCES

[1]I. Ehican and B. Sarioglu, in *11th International Conference on Electrical and Electronics Engineering (ELECO)* (IEEE, 2019), p. 397.
[2]S. Jeong, Y. Chen, T. Jang, J. M. L. Tsai, D. Blaauw, H. S. Kim, and D. Sylvester, IEEE J. Solid-State Circuits **53**(1), 261 (2018).
[3]S. H. Kang, V. Rajaram, S. D. Calisgan, A. Risso, Z. Y. Qian, and M. Rinaldi, in *Proceedings of IEEE International Conference on Microelectromechanical Systems* (IEEE, 2021), p. 144.
[4]Q. P. Chi, H. R. Yan, C. Zhang, Z. B. Pang, and L. D. Xu, IEEE Trans. Indus. Inform. **10**(2), 1417 (2014).
[5]C. Bersani, A. Ouammi, R. Sacile, and E. Zero, Energies **13**(14), 3647 (2020).
[6]J. Rabaey, in *Proceedings of Technical Program: 2009 International Symposium on VLSI Technology Systems and Applications* (IEEE, 2009), p. 42.
[7]R. H. Olsson, C. Gordon, and R. Bogoslovov, J. Phys. Conf. Ser. **1407**, 012042 (2019).
[8]G. Saldamli, S. Deshpande, K. Jawalekar, P. Gholap, L. Tawalbeh, and L. Ertaul, in *4th International Conference on Fog and Mobile Edge Computing (FMEC)* (IEEE, 2019), p. 229.
[9]L. Shu, M. Mukherjee, X. L. Xu, K. Wang, and X. L. Wu, IEEE Access **4**, 1700 (2016).
[10]M. Ahmed, T. Dankwort, S. Grunzig, V. Lange, and B. Gojdka, Micromachines (Basel) **13**(3), 407 (2022).
[11]Y. Z. Han, G. Z. Xuan, J. H. Zhao, and Z. You, Micromachines (Basel) **13**(8), 1333 (2022).
[12]X. Z. Liu, N. J. Qi, K. R. Dai, Y. J. Yin, J. H. Zhao, X. F. Wang, and Z. You, Energy **239**, 122368 (2022).
[13]W. Z. Zhu, T. Wu, G. F. Chen, C. Cassella, M. Assylbekova, M. Rinaldi, and N. McGruer, IEEE Sens. J. **18**(24), 9902 (2018).
[14]A. Bannoura, F. Hoflinger, O. Gorgies, G. U. Gamm, J. Albesa, and L. M. Reindl, Electronics **5**(1), 4 (2016).
[15]R. La Rosa, C. Trigona, B. Ando', and S. Baglio, in *IEEE Metroind4.0&IoT* (IEEE, 2019), p. 12.
[16]U. Dudko and L. Overmeyer, IEEE Sens. J. **21**(3), 3225 (2021).
[17]Z. Qian, S. Kang, V. Rajaram, C. Cassella, N. E. McGruer, and M. Rinaldi, Nat. Nanotechnol. **12**(10), 969 (2017).
[18]V. Rajaram, Z. Y. Qian, S. H. Kang, S. D. Calisgan, N. E. McGruer, and M. Rinaldi, IEEE Sens. J. **18**(19), 7833 (2018).
[19]A. Risso, V. Rajaram, S. Kang, S. D. Calisgan, M. M. Pavese, Z. Y. Qian, and M. Rinaldi, Sci. Rep. **12**(1), 12603 (2022).
[20]Z. Y. Wang, J. D. Zhang, X. G. Wu, M. Birau, G. M. Yu, H. G. Yu, Y. H. Qi, P. Desjardins, X. S. Meng, J. P. Gao, E. Todd, N. H. Song, Y. M. Bai, A. M. R. Beaudin, and G. LeClair, Pure Appl. Chem. **76**(7-8), 1435 (2004).
[21]W. Guo, Y. Liu, and T. Han, Opt. Express **24**(18), 20586 (2016).
[22]T. D. Dao, K. Chen, S. Ishii, A. Ohi, T. Nabatame, M. Kitajima, and T. Nagao, ACS Photonics **2**(7), 964 (2015).
[23]N. Liu, M. Mesch, T. Weiss, M. Hentschel, and H. Giessen, Nano Lett. **10**(7), 2342 (2010).
[24]M. R. Rakhshani, IEEE Sens. J. **20**(23), 14166 (2020).
[25]Y. Han and N. Shikazono, Int. J. Multiphase Flow **35**(10), 896 (2009).